

DISCRETE CONTRASTIVE DIFFUSION FOR CROSS-MODAL MUSIC AND IMAGE GENERATION

Ye Zhu

Department of Computer Science
Illinois Institute of Technology
Chicago, IL 60616, USA
yzhu96@hawk.iit.edu

Yu Wu

School of Computer Science
Wuhan University
Wuhan 430000, China
wuyucs@whu.edu.cn

Kyle Olszewski, Jian Ren, Sergey Tulyakov

Snap Inc.
Santa Monica, CA 90405, USA
{kolszewski, jren, stulyakov}@snap.com

Yan Yan

Department of Computer Science
Illinois Institute of Technology
Chicago, IL 60616, USA
yyan34@iit.edu

ABSTRACT

Diffusion probabilistic models (DPMs) have become a popular approach to conditional generation, due to their promising results and support for cross-modal synthesis. A key desideratum in conditional synthesis is to achieve high correspondence between the conditioning input and generated output. Most existing methods learn such relationships implicitly, by incorporating the prior into the variational lower bound. In this work, we take a different route—we explicitly enhance input-output connections by maximizing their mutual information. To this end, we introduce a *Conditional Discrete Contrastive Diffusion (CDCD)* loss and design two contrastive diffusion mechanisms to effectively incorporate it into the denoising process, combining the diffusion training and contrastive learning for the first time by connecting it with the conventional variational objectives. We demonstrate the efficacy of our approach in evaluations with diverse multimodal conditional synthesis tasks: dance-to-music generation, text-to-image synthesis, as well as class-conditioned image synthesis. On each, we enhance the input-output correspondence and achieve higher or competitive general synthesis quality. Furthermore, the proposed approach improves the convergence of diffusion models, reducing the number of required diffusion steps by more than 35% on two benchmarks, significantly increasing the inference speed.

1 INTRODUCTION

Generative tasks that seek to synthesize data in different modalities, such as audio and images, have attracted much attention. The recently explored diffusion probabilistic models (DPMs) Sohl-Dickstein et al. (2015b) have served as a powerful generative backbone that achieves promising results in both unconditional and conditional generation Kong et al. (2020); Mittal et al. (2021); Lee & Han (2021); Ho et al. (2020); Nichol & Dhariwal (2021); Dhariwal & Nichol (2021); Ho et al. (2022); Hu et al. (2021). Compared to the unconditional case, conditional generation is usually applied in more concrete and practical cross-modality scenarios, *e.g.*, video-based music generation Di et al. (2021); Zhu et al. (2022a); Gan et al. (2020a) and text-based image generation Gu et al. (2022); Ramesh et al. (2021); Li et al. (2019); Ruan et al. (2021). Most existing DPM-based conditional synthesis works Gu et al. (2022); Dhariwal & Nichol (2021) learn the connection between the conditioning and the generated data implicitly by adding a prior to the variational lower bound Sohl-Dickstein et al. (2015b). While such approaches still feature high generation fidelity, the correspondence between the conditioning and the synthesized data can sometimes get lost, as illustrated in the right column in Fig. 1. To this end, we aim to explicitly enhance the input-output faithfulness via their maximized mutual information under the diffusion generative framework for conditional settings in this paper. Examples of our synthesized music audio and image results are given in Fig. 1.

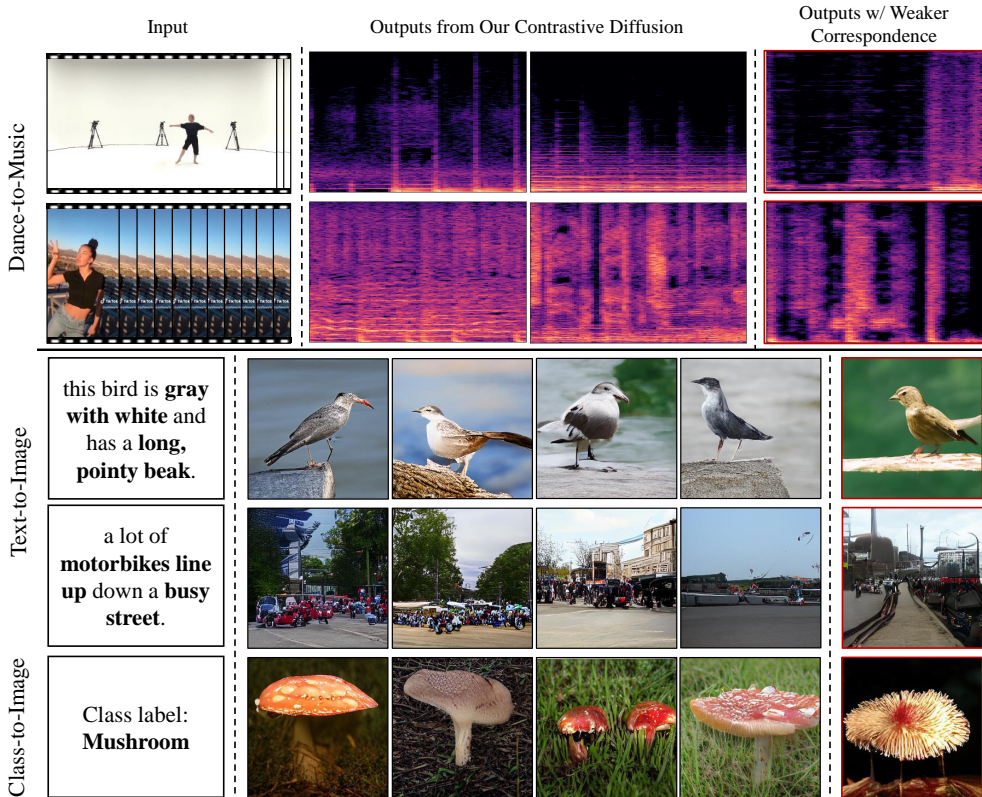


Figure 1: Examples of the input (left column) and synthesized output (middle column) from our contrastive diffusion model for dance-to-music (Rows 1-2), text-to-image (Rows 3-4), and class-conditioned (Row 5) generation experiments on five datasets. The right column shows some synthesized data with reasonable quality but weaker correspondence to the input from existing methods Zhu et al. (2022a); Gu et al. (2022).

Contrastive methods Oord et al. (2018); Bachman et al. (2019); Song & Ermon (2020a) have been proven to be very powerful for data representation learning. Their high-level idea aims to learn the representation z of raw data x based on the assumption that a properly encoded z benefits the ability of a generative model p to reconstruct the raw data given z as prior. This idea can be achieved via optimization of the density ratio $\frac{p(x|z)}{p(x)}$ Oord et al. (2018) as an entirety, without explicitly modeling the actual generative model p . While the direct optimization of mutual information via generative models p is a challenging problem to implement and train Song & Ermon (2020b); Belghazi et al. (2018) in the conventional contrastive representation learning field, we show that this can be effectively done within our proposed contrastive diffusion framework. Specifically, we reformulate the optimization problem for the desired conditional generative tasks via DPMs by analogy to the above embedding z and raw data x with our conditioning input and synthesized output. We introduce a *Conditional Discrete Contrastive Diffusion (CDCD)* loss, and design two contrastive diffusion mechanisms - *step-wise parallel diffusion* that invokes multiple parallel diffusion processes during contrastive learning, and *sample-wise auxiliary diffusion*, which maintains one principal diffusion process, to effectively incorporate the *CDCD* loss into the denoising process. We demonstrate that with the proposed contrastive diffusion method, we can not only effectively train so as to maximize the desired mutual information by connecting the *CDCD* loss with the conventional variational objective function, but also to directly optimize the generative network p . The optimized *CDCD* loss further encourages faster convergence of a DPM model with fewer diffusion steps. We additionally present our *intra-* and *inter-*negative sampling methods by providing internally disordered and instance-level negative samples, respectively.

To better illustrate the input-output connections, we conduct main experiments on the novel cross-modal dance-to-music generation task Zhu et al. (2022a), which aims to generate music audio based on silent dance videos. Compared to other tasks such as text-to-image synthesis, dance-to-music

generation explicitly evaluates the input-output correspondence in terms of various cross-modal alignment features such as dance-music beats, genre and general quality. However, various generative settings, frameworks, and applications can also benefit from our contrastive diffusion approach, *e.g.*, joint or separate training of conditioning encoders, continuous or discrete conditioning inputs, and diverse input-output modalities as detailed in Sec. 4. Overall, we achieve results superior or comparable to state-of-the-art on three conditional synthesis tasks: dance-to-music (datasets: AIST++ Tsuchida et al. (2019); Li et al. (2021), TikTok Dance-Music Zhu et al. (2022a)), text-to-image (datasets: CUB200 Wah et al. (2011), MSCOCO Lin et al. (2014)) and class-conditioned image synthesis (dataset: ImageNet Russakovsky et al. (2015)). Our experimental findings suggest three key take-away: ① Improving the input-output connections via maximized mutual information is indeed beneficial for their correspondence and the general fidelity of the results (see Fig. 1 and supplement). ② Both our proposed *step-wise parallel diffusion* with *intra*-negative samples and *sample-wise auxiliary diffusion* with *inter*-negative samples show state-of-the-art scores in our evaluations. The former is more beneficial for capturing the intra-sample correlations, *e.g.*, musical rhythms, while the latter improves the instance-level performance, *e.g.*, music genre and image class. ③ With maximized mutual information, our conditional contrastive diffusion *converge in substantially fewer diffusion steps* compared to vanilla DPMs, while maintaining the same or even superior performance (approximately **35%** fewer steps for dance-to-music generation and **40%** fewer for text-to-image synthesis), thus significantly increasing inference speed.

2 BACKGROUND

Diffusion Probabilistic Models. DPMs Sohl-Dickstein et al. (2015b) are a class of generative models that learn to convert a simple Gaussian distribution into a data distribution. This process consists of a forward *diffusion* process and a reverse *denoising* process, each consisting of a sequence of T steps that act as a Markov chain. During forward diffusion, an input data sample x_0 is gradually “corrupted” at each step t by adding Gaussian noise to the output of step $t - 1$. The reverse denoising process, seeks to convert the noisy latent variable x_T into the original data sample x_0 by removing the noise added during diffusion. The stationary distribution for the final latent variable x_T is typically assumed to be a normal distribution, $p(x_T) = \mathcal{N}(x_T|0, \mathbf{I})$.

An extension of this approach replaces the continuous state with a discrete one Sohl-Dickstein et al. (2015a); Hooeboom et al. (2021); Austin et al. (2021), in which the latent variables $x_{1:T}$ typically take the form of one-hot vectors with K categories. The diffusion process can then be parameterized using a multinomial categorical transition matrix defined as $q(x_t|x_{t-1}) = \text{Cat}(x_t; p = x_{t-1}Q_t)$, where $[Q_t]_{ij} = q(x_t = j|x_{t-1} = i)$. The reverse process $p_\theta(x_t|x_{t-1})$ can also be factorized as conditionally independent over the discrete sequences Austin et al. (2021).

In both the continuous and discrete state formulations of DPMs Song & Ermon (2020c); Song et al. (2020b); Kingma et al. (2021); Song et al. (2021); Huang et al. (2021); Vahdat et al. (2021), the denoising process p_θ can be optimized by the KL divergence between q and p_θ in closed forms Song et al. (2020a); Nichol & Dhariwal (2021); Ho et al. (2020); Hooeboom et al. (2021); Austin et al. (2021) via the variational bound on the negative log-likelihood:

$$\mathcal{L}_{\text{vb}} = \mathbb{E}_q[\underbrace{D_{\text{KL}}(q(x_T|x_0)||p(x_T))}_{\mathcal{L}_T} + \sum_{t>1} \underbrace{D_{\text{KL}}(q(x_{t-1}|x_t, x_0)||p_\theta(x_{t-1}|x_t))}_{\mathcal{L}_{t-1}} - \underbrace{\log p_\theta(x_0|x_1)}_{\mathcal{L}_0}]. \quad (1)$$

Existing conditional generation works via DPMs Gu et al. (2022); Dhariwal & Nichol (2021) usually learn the implicit relationship between the conditioning c and the synthesized data x_0 by directly adding the c as the prior in (1). DPMs with discrete state space provide more controls on the data corruption and denoising compared to its continuous counterpart Austin et al. (2021); Gu et al. (2022) by the flexible designs of transition matrix, which benefits for practical downstream operations such as editing and interactive synthesis Tseng et al. (2020); Cui et al. (2021); Xu et al. (2021). We hence employ contrastive diffusion using a discrete state space in this work.

Contrastive Representation Learning. Contrastive learning uses loss functions designed to make neural networks learn to understand and represent the specific similarities and differences between elements in the training data without labels explicitly defining such features, with *positive* and *negative* pairs of data points, respectively. This approach has been successfully applied in learning representations of high-dimensional data Oord et al. (2018); Bachman et al. (2019); He et al. (2020); Song & Ermon (2020a); Chen et al. (2020); Lin et al. (2021). Many such works seek to maximize the

mutual information between the original data x and its learned representation z under the framework of likelihood-free inference Oord et al. (2018); Song & Ermon (2020a); Wu et al. (2021). The above problem can be formulated as maximizing a density ratio $\frac{p(x|z)}{p(x)}$ that preserves the mutual information between the raw data x and learned representation z .

To achieve this, existing contrastive methods Oord et al. (2018); Durkan et al. (2020); He et al. (2020); Zhang et al. (2021) typically adopt a neural network to directly model the ratio as an entirety and avoid explicitly considering the actual generative model $p(x|z)$, which has proven to be a more challenging problem Song & Ermon (2020b); Belghazi et al. (2018). In contrast, we show that by formulating the conventional contrastive representation learning problem under the generative setting, the properties of DPMs enable us to directly optimize the model p in this work, which can be interpreted as the optimal version of the density ratio Oord et al. (2018).

Vector-Quantized Representations for Conditional Generation. Vector quantization is a classical technique in which a high-dimensional space is represented using a discrete number of vectors. More recently, Vector-Quantized (VQ) deep learning models employ this technique to allow for compact and discrete representations of music and image data Oord et al. (2017); Razavi et al. (2019); Esser et al. (2021b); Dhariwal et al. (2020); Chen et al. (2022). Typically, the VQ-based models use an encoder-codebook-decoder framework, where the “codebook” contains a fixed number of vectors (entries) to represent the original high dimensional raw data. The encoder transforms the input x into feature embedding that are each mapped to the closest corresponding vector in the codebook, while the decoder uses the set of quantized vectors z to reconstruct the input data, producing x' as illustrated in the upper part of Fig. 2.

In this work, we perform conditional diffusion process on the VQ space (*i.e.*, discrete token sequences) as shown in the bottom part of Fig. 2, which largely reduces the dimensionality of the raw data, thus avoiding the expensive raw data decoding and synthesis. As our approach is flexible enough to be employed with various input and output modalities, the exact underlying VQ model we use depends on the target data domain. For music synthesis, we employ a fine-tuned Jukebox Dhariwal et al. (2020) model, while for image generation, we employ VQ-GAN Esser et al. (2021b). See Sec. 4 for further details. We refer to z , the latent quantized representation of x , as z_0 below to distinguish it from the latent representation at prior stages in the denoising process.

3 METHOD

Here we outline our approach to cross-modal and conditional generation using our proposed discrete contrastive diffusion approach, which is depicted in Fig. 2. In Sec. 3.1, we formulate our Conditional Discrete Contrastive Diffusion loss in detail, and demonstrate how it helps to maximize the mutual information between the conditioning and generated discrete data representations. Sec. 3.2 defines two specific mechanisms for applying this loss within a diffusion model training framework, *sample-wise* and *step-wise*. In Sec. 3.3, we detail techniques for constructing negative samples designed to improve the overall quality and coherence of the generated sequences.

Given the data pair (c, x) , where c is the conditioning information from a given input modality (*e.g.*, videos, text, or a class label), our objective is to generate a data sample x in the target modality (*e.g.*, music audio or images) corresponding to c . In the training stage, we first employ and train a VQ-based model to obtain discrete representation z_0 of the data x from the target modality. Next, our diffusion process operates on the encoded latent representation z_0 of x . The denoising process recovers the latent representation z_0 given the conditioning c that can be decoded to obtain the reconstruction x' . In inference, we generate z_0 based on the conditioning c , and decode the latent VQ representation z_0 back to raw data domain using the decoder from the pre-trained and fixed VQ decoder.

3.1 CONDITIONAL DISCRETE CONTRASTIVE DIFFUSION LOSS

We seek to enhance the connection between c and the generated data z_0 by maximizing their mutual information, defined as $I(z_0; c) = \sum_{z_0} p_\theta(z_0, c) \log \frac{p_\theta(z_0|c)}{p_\theta(z_0)}$. We introduce a set of negative VQ sequences $Z' = \{z^1, z^2, \dots, z^N\}$, encoded from N negative samples $X' = \{x^1, x^2, \dots, x^N\}$, and define $f(z_0, c) = \frac{p_\theta(z_0|c)}{p_\theta(z_0)}$. Our proposed Conditional Discrete Contrastive Diffusion (CDCD) loss is:

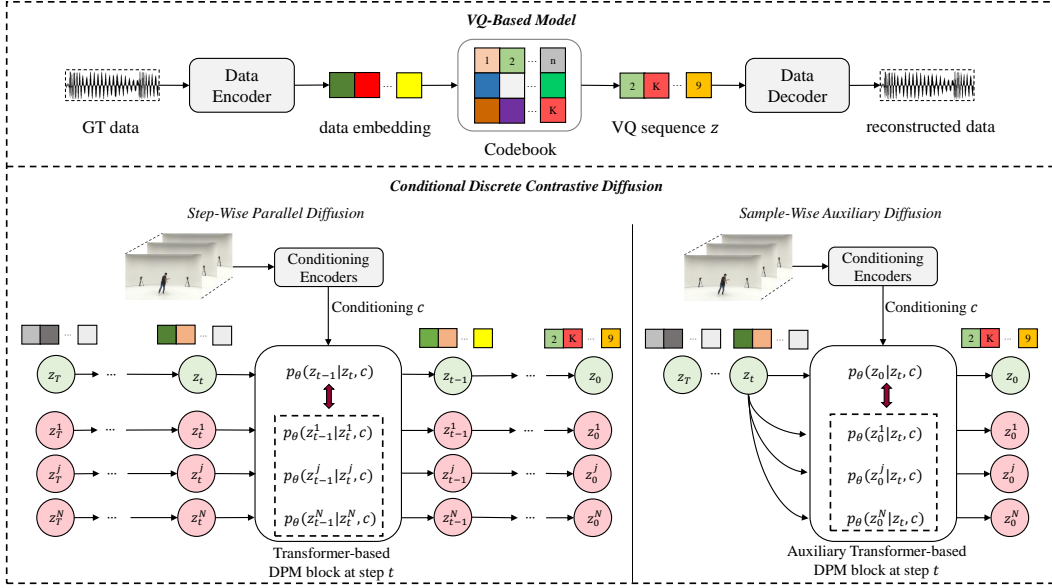


Figure 2: **Overview of the proposed pipeline.** Our framework includes two major components: a VQ-based encoder-decoder model (top) and a conditioned discrete contrastive diffusion as generative model on the VQ space (bottom). In the contrastive diffusion stage, we illustrate our proposed step-wise parallel diffusion (bottom left) and sample-wise auxiliary diffusion (bottom right). The variables in green denote those from the principal diffusion process, while the variables in red represent the diffusion invoked by negative samples. Here we show audio generation from video input, but demonstrate that this approach extends to different modalities, *e.g.*, text-to-image.

$$\mathcal{L}_{\text{CDCD}} := -\mathbb{E} \left[\log \frac{f(z_0, c)}{f(z_0, c) + \sum_{z^j \in Z'} f(z_0^j, c)} \right]. \quad (2)$$

The proposed *CDCD* loss is similar to the categorical cross-entropy loss for classifying the positive sample as in Oord et al. (2018), where our conditioning c and the generated data z_0 corresponds to the original learned representation and raw data, and optimization of this loss leads to maximization of $I(z_0; c)$. However, the loss in Oord et al. (2018) models the density ratio $f(z_0, c)$ as an entirety. In our case, we demonstrate that the DPMs properties Sohl-Dickstein et al. (2015b); Ho et al. (2020); Austin et al. (2021) enable us to directly optimize the actual distribution p_θ within the diffusion process for the desired conditional generation tasks. Specifically, we show the connections between the proposed *CDCD* loss and the conventional variational loss \mathcal{L}_{vb} (see (1)) in Sec. 3.2, and thus how it contributes to efficient DPM learning. Additionally, we can derive the lower bound for the mutual information as $I(z_0; c) \geq \log(N) - \mathcal{L}_{\text{CDCD}}$ (see supplement for details), which indicates that a larger number of negative samples increases the lower bound. These two factors allow for *faster* convergence of a DPM with *fewer* diffusion steps.

3.2 PARALLEL AND AUXILIARY DIFFUSION PROCESS

The *CDCD* loss in (2) considers the mutual information between c and z_0 in a general way, without specifying the intermediate diffusion steps. We propose and analyze two contrastive diffusion mechanisms to efficiently incorporate this loss into DPM learning, and demonstrate that we can directly optimize the generative model p_θ in the diffusion process. We present our *step-wise parallel diffusion* and the *sample-wise auxiliary diffusion* mechanisms, which are distinguished by the specific operations applied for the intermediate negative latent variables $z_{1:T}^j$ for each negative sample x^j . The high-level intuition for the parallel and auxiliary designs is to emphasize different attributes of the synthesized data given specific applications. Particularly, we propose the parallel variant to learn the internal coherence of the audio sequential data by emphasizing the gradual change at each time step, while the auxiliary mechanism focuses more on the sample-level connections to the conditioning.

Step-Wise Parallel Diffusion. This mechanism not only focuses on the mutual information between c and z_0 , but also takes the intermediate negative latent variables $z_{1:T}^j$ into account by explicitly invoking the complete diffusion process for each negative sample $z^j \in Z'$. As illustrated in Fig. 2 (bottom left), we initiate $N + 1$ parallel diffusion processes, among which N are invoked by negative samples. For each negative sample $x^j \in X'$, we explicitly compute its negative latent discrete variables $z_{0:T}^j$. In this case, (2) is as follows (see supplement for the detailed derivation):

$$\mathcal{L}_{\text{CD}CD\text{-Step}} := \mathbb{E}_Z \log \left[1 + \frac{p_\theta(z_{0:T})}{p_\theta(z_{0:T}|c)} N \mathbb{E}_{Z'} \left[\frac{p_\theta(z_{0:T}^j|c)}{p_\theta(z_{0:T}^j)} \right] \right] \equiv \mathcal{L}_{\text{vb}}(z, c) - C \sum_{z^j \in Z'} \mathcal{L}_{\text{vb}}(z^j, c). \quad (3)$$

The equation above factorizes the proposed *CD**CD* loss using the step-wise parallel diffusion mechanism into two terms, where the first term corresponds to the original variational bound \mathcal{L}_{vb} , and the second term can be interpreted as the negative sum of variational bounds induced by the negative samples and the provided conditioning c . C is a constant as detailed in our supplement.

Sample-Wise Auxiliary Diffusion. Alternatively, our *sample-wise auxiliary diffusion* mechanism maintains one principal diffusion process, as in traditional diffusion training, shown in Fig. 2 (bottom right). It contrasts the intermediate *positive* latent variables $z_{1:T}$ with the negative sample $z_0^j \in Z$. In this case, we can write the *CD**CD* loss from (2) as (see supplement for details):

$$\mathcal{L}_{\text{CD}CD\text{-Sample}} := \mathbb{E}_q[-\log p_\theta(z_0|z_t, c)] - C \sum_{z^j \in Z'} \mathbb{E}_q[-\log p_\theta(z_0^j|z_t, c)]. \quad (4)$$

As with the step-wise loss, the *CD**CD*-*Sample* loss includes two terms. The first refers to sampling directly from the positive z_0 at an arbitrary timestep t . The second sums the same auxiliary loss from negative samples z_0^j . This marginalization operation is based on the property of Markov chain as in previous discrete DPMs Austin et al. (2021); Gu et al. (2022), which imposes direct supervision from the sample data. The first term is similar to the auxiliary denoising objective in Austin et al. (2021); Gu et al. (2022).

Both contrastive diffusion mechanisms enable us to effectively incorporate the *CD**CD* loss into our DPM learning process by directly optimizing the actual denoising generative network p_θ .

Final Loss Function. The final loss function for our contrastive diffusion training process is:

$$\mathcal{L} = \mathcal{L}_{\text{vb}}(z, c) + \lambda \mathcal{L}_{\text{CD}CD}, \quad (5)$$

\mathcal{L}_{vb} is conditioning c related, and takes the form of $\mathcal{L}_{t-1} = D_{\text{KL}}(q(z_{t-1}|z_t, z_0) || p_\theta(z_{t-1}|z_t, c))$ as in Gu et al. (2022), where c included as the prior for all the intermediate steps. $\mathcal{L}_{\text{CD}CD}$ refers to either the step-wise parallel diffusion or sample-wise auxiliary diffusion loss. Empirically, we can omit the first term in (3), or directly optimize $\mathcal{L}_{\text{CD}CD\text{-Step}}$, in which the standard \mathcal{L}_{vb} is already included. The detailed training algorithm is explained in the supplement.

3.3 INTRA- AND INTER-NEGATIVE SAMPLING

Previous contrastive works construct negative samples using techniques such as image augmentation Chen et al. (2020); He et al. (2020) or spatially adjacent image patches Oord et al. (2018). In this work, we categorize our sampling methods into *intra*- and *inter*-negative samplings as in Fig. 3. For the *intra*-sample negative sampling, we construct X' based on the given original x . This bears resemblance to the patch-based technique in the image domain Oord et al. (2018). As for the audio data, we first divide the original audio waveform into multiple chunks, and randomly shuffle their ordering. For the *inter*-sample negative sampling, X' consists of instance-level negative samples x' that differ from the given data pair (c, x) . In practice, we define negative samples x' to be music sequences with different musical genres from x in the music generation task, while x' denotes images other than x in the image synthesis task (in practice, we choose x' with different class labels as x).

Based on our proposed contrastive diffusion modes and negative sampling methods, there are four possible contrastive settings: step-wise parallel diffusion with either *intra*- or *inter*-negative sampling (denoted as *Step-Intra* and *Step-Inter*), or sample-wise auxiliary diffusion with either *intra*- or *inter*-negative sampling (denoted as *Sample-Intra* and *Sample-Inter*). Intuitively, we argue that *Step-Intra* and *Sample-Inter* settings are more reasonable compared to *Step-Inter* and *Sample-Intra* because of the consistency between the diffusion data corruption process and the way to construct negative samples. Specifically, the data corruption process in the discrete DPMs includes sampling and

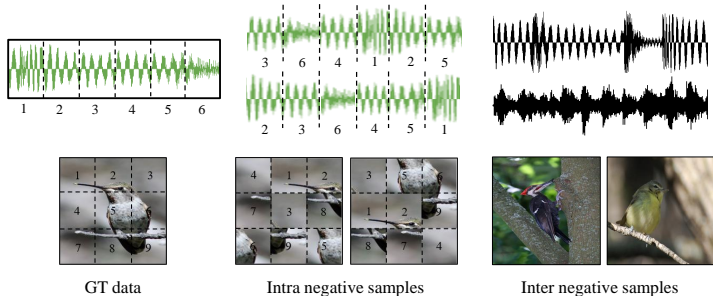


Figure 3: Illustration of *intra*- and *inter*-negative sampling for music and image data.

replacing certain tokens with some random or mask tokens at each diffusion step Austin et al. (2021); Gu et al. (2022), which is a chunk-level operation within a given data sequence similar to the ways we construct *intra*-negative samples by shuffling the chunk-level orders. In contrast, the *sample-wise auxiliary diffusion* seeks to provide sample-level supervision, which is consistent with our *inter*-negative sampling method.

In the interest of clarity and concision, we only present the experimental results for *Step-Intra* and *Sample-Inter* settings in Sec. 4 of our main paper. The complete results obtained with other contrastive settings and more detailed analysis are included in the supplement.

4 EXPERIMENTS

We conduct experiments on three conditional generation tasks: dance-to-music generation, text-to-image synthesis, and class-conditioned image synthesis. For the dance-to-music task, we seek to generate audio waveforms for complex music from human motion and dance video frames. For the text-to-image task, the objective is to generate images from given textual descriptions. Given our emphasis on the input-output faithfulness for cross-modal generations, the main analysis are based on the dance-to-music generation task since the evaluation protocol from Zhu et al. (2022a) explicitly measures such connections in terms of beats, genre and general correspondence for generated music.

4.1 DANCE-TO-MUSIC GENERATION

Dataset. We use the AIST++ Li et al. (2021) dataset and the TikTok Dance-Music dataset Zhu et al. (2022a) for the dance-to-music experiments. AIST++ is a subset of the AIST dataset Tsuchida et al. (2019), which contains 1020 dance videos and 60 songs performed by professional dancers and filmed in clean studio environment settings without occlusions. AIST++ provide human motion data in the form of SMPL Loper et al. (2015) parameters and body keypoints, and includes the annotations for different genres and choreography styles. The TikTok Dance-Music dataset includes 445 dance videos collected from the social media platform. The 2D skeleton data extracted with OpenPose Cao et al. (2017); Cao et al. (2019) is used as the motion representation. We adopt the official cross-modality splits without overlapping music songs for both datasets.

Implementations. The sampling rate for all audio signals is 22.5 kHz in our experiments. We use 2-second music samples as in Zhu et al. (2022a) for the main experiments. We fine-tuned the pre-trained Jukebox Dhariwal et al. (2020) for our Music VQ-VAE model. For the motion encoder, we deploy a backbone stacked with convolutional layers and residual blocks. For the visual encoder, we extract I3D features Carreira & Zisserman (2017) using a model pre-trained on Kinetics Kay et al. (2017) as the visual conditioning. The motion and visual encoder outputs are concatenated to form the final continuous conditioning input to our contrastive diffusion model. For the contrastive diffusion model, we adopt a transformer-based backbone to learn the denoising network p_θ . It includes 19 transformer blocks, with each block consisting of full attention, cross attention and feed forward modules, and a channel size of 1024 for each block. We set the initial weight for the contrastive loss as $\lambda = 5e - 5$. The number N of intra- and inter-negative samples for each GT music sample is 10. The visual encoder, motion encoder, and the contrastive diffusion model are jointly optimized. More implementation details are provided in the supplement.

Evaluations. The evaluation of synthesized music measures both the conditioning-output correspondence and the general synthesis quality using the metrics introduced in Zhu et al. (2022a). Specifically,

Table 1: Quantitative evaluation results for the dance-to-music task on the AIST++ dataset. This table shows the best performance scores we obtain for different contrastive diffusion steps. We report the mean and standard deviations of our contrastive diffusion for three inference tests.

Musical features	Rhythms	Rhythms	Genre	Coherence	Quality
Metrics	Coverage \uparrow	Hit \uparrow	Accuracy \uparrow	MOS \uparrow	MOS \uparrow
GT Music	100	100	88.5	4.7	4.8
Foley	74.1	69.4	8.1	2.9	-
Dance2Music	83.5	82.4	7.0	3.0	-
CMT	85.5	83.5	11.6	3.0	-
D2M-GAN	88.2	84.7	24.4	3.3	3.4
Ours Vanilla	89.0 \pm 1.1	83.8 \pm 1.5	25.3 \pm 0.8	3.3	3.6
Ours Step-Intra	93.9\pm1.2	90.7\pm1.5	25.8 \pm 0.6	3.6	3.5
Ours Sample-Inter	91.8 \pm 1.6	86.9 \pm 1.4	27.2\pm0.5	3.6	3.6

Table 2: Quantitative evaluation results for the dance-to-music task on the TikTok dataset. We set the default number of diffusion steps to be 80.

Methods	Beats Coverage/Hit \uparrow
D2M-GAN	88.4/ 82.3
Ours Vanilla	88.7/ 81.4
Ours Step-Intra	91.8/ 86.3
Ours Sample-Inter	90.1/ 85.5

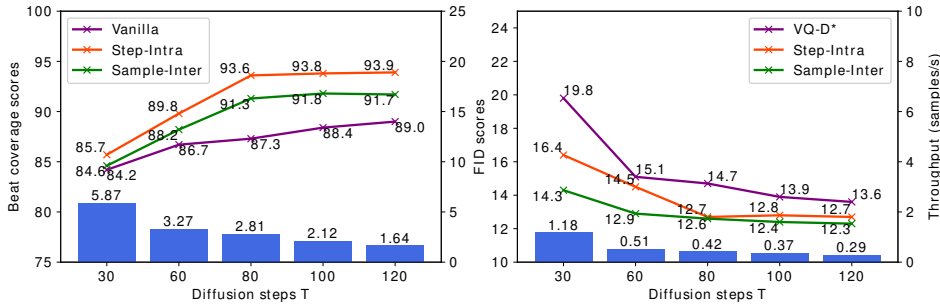


Figure 4: Convergence analysis in terms of diffusion steps for the dance-to-music task on AIST++ dataset (left) and the text-to-image task on CUB200 dataset (right). We observe that our contrastive diffusion models converge at around 80 steps and 60 steps, resulting 35% steps and 40% steps less compared to the vanilla models that converge at 120 steps and 100 steps, while maintaining superior performance, respectively. We use the same number of steps for training and inference.

the metrics include the beats coverage score, the beats hit scores, the genre accuracy score, and two subjective evaluation tests with Mean Opinion Scores (MOS) for the musical coherence and general quality. Among these metrics, the beats scores emphasize the intra-sample properties, since they calculate the second-level audio onset strength within musical chunks Ellis (2007), while the genre accuracy focuses on the instance-level musical attributes of music styles. Detailed explanations of the above metrics can be found in Zhu et al. (2022a). We compare against multiple dance-to-music generation works: Foley Gan et al. (2020a), Dance2Music Aggarwal & Parikh (2021), CMT Di et al. (2021), and D2M-GAN Zhu et al. (2022a). The first three models rely on symbolic discrete MIDI musical representations, while the last one also uses a VQ musical representation. The major difference between the symbolic MIDI and discrete VQ musical representations lies within the fact that the MIDI is pre-defined for each instrument, while the VQ is learning-based. The latter thus enables complex and free music synthesis appropriate for scenarios like dance videos.

Results and Discussion. The quantitative experimental results are shown in Tab. 1 and Tab. 2. Our proposed methods achieve better performance than the competing methods even with vanilla version without contrastive mechanisms. Furthermore, we find that the *Step-Intra* setting is more helpful in increasing the beats scores, while the *Sample-Inter* setting yields more improvements for the genre accuracy scores. We believe this is due to the evaluation methods of different metrics. The beats scores measure the chunk-level (*i.e.*, the audio onset strength Ellis (2007)) consistency between the GT and synthesized music samples Zhu et al. (2022a), while the genre scores consider the overall musical attributes of each sample sequence in instance level. This finding is consistent with our assumptions in Sec. 3.3.

Convergence Analysis. We also analyze the impact of the proposed contrastive diffusion on model convergence in terms of diffusion steps. The number of diffusion steps is a significant hyper-parameter for DPMs Sohl-Dickstein et al. (2015b); Nichol & Dhariwal (2021); Austin et al. (2021); Gu et al. (2022); Kingma et al. (2021) that directly influences the inference time and synthesis quality. Previous works have shown that a larger number of diffusion steps usually lead to better model performance, but longer inference times Kingma et al. (2021); Gu et al. (2022). We demonstrate that, with the

Table 3: FID and CLIPScore for text-to-image synthesis on CUB-200 and MSCOCO datasets. The VQ-D model with * shows the results we reproduced by training using the original code, which can be considered as our baseline. We show the results obtained with default 80 diffusion steps in both training and inference.

Datasets	CUB-200		MSCOCO	
	FID ↓	CLIPScore ↑	FID ↓	CLIPScore ↑
StackGAN	51.89	-	74.05	-
StackGAN++	15.30	-	81.59	-
SEGAN	18.17	-	32.28	-
AttnGAN	23.98	-	35.49	65.66
DM-GAN	16.09	-	32.64	65.45
DF-GAN	14.81	-	21.42	66.42
DAE-GAN	15.19	-	28.12	-
DALLE	56.10	74.66	27.50	-
VQ-D (T=100)	12.97	-	30.17	-
VQ-D* (T=80)	14.61	74.96	36.45	65.53
Ours Step-Intra (T=80)	12.73	75.32	32.25	66.22
Ours Sample-Inter (T=80)	12.61	75.50	28.76	66.79

Table 4: FID scores and top 5 classification accuracy using pre-trained ResNet101 He et al. (2016) for class-conditioned image synthesis on ImageNet 256×256 . Our model follows the *Sample-Inter* contrastive setting with 80 diffusion steps in both training and inference.

Methods	FID ↓	Acc. ↑
ImageBART	21.19	-
VQGAN	15.78	-
IDDP	12.30	-
VQ-D (T=100)	11.89	72.72
Ours (T=80)	11.74	77.63

improved mutual information via the proposed contrastive diffusion method, we can greatly reduce the number of steps needed. As shown in Fig. 4 (left), we observe that the beats scores reach a stable level at approximately 80 steps, $\sim 35\%$ less than the vanilla DPM that converges in ~ 120 steps. More ablation studies and analysis on this task can be found in the supplement.

4.2 CONDITIONAL IMAGE SYNTHESIS

Dataset. We conduct text-to-image synthesis on CUB200 Wah et al. (2011) and MSCOCO datasets Lin et al. (2014). The CUB200 dataset contains images of 200 bird species. Each image has 10 corresponding text descriptions. The MSCOCO dataset contains 82k images for training and 40k images for testing. Each image has 5 text descriptions. We also perform the class-conditioned image generation on ImageNet Deng et al. (2009); Russakovsky et al. (2015). Implementation details for both tasks are provided in the supplement.

Evaluations. We adopt two evaluation metrics for text-to-image synthesis: the classic FID score Heusel et al. (2017) as the general measurement for image quality, and the CLIPScore Hessel et al. (2021) to evaluate the correspondence between the given textual caption and the synthesized image. For the class-conditioned image synthesis, we use the FID score and a classifier-based accuracy for general and input-output correspondence measurement. We compare against text-to-image generation methods including StackGAN Zhang et al. (2017), StackGAN++ Zhang et al. (2018), SEGAN Tan et al. (2019), AttnGAN Xu et al. (2018), DM-GAN Zhu et al. (2019), DF-GAN Tao et al. (2020), DAE-GAN Ruan et al. (2021), DALLE Ramesh et al. (2021), and VQ-Diffusion Gu et al. (2022). For experiments on ImageNet, we list the result comparisons with ImageBART Esser et al. (2021a), VQGAN Esser et al. (2021b), IDDP Nichol & Dhariwal (2021), and VQ-D Gu et al. (2022). Specifically, VQ-Diffusion Gu et al. (2022) also adopts the discrete diffusion generative backbone, which can be considered as the vanilla version without contrastive mechanisms. Additionally, we provide more comparisons with other methods in terms of dataset, model scale and training time in the supplement for a more comprehensive and fair understanding of our proposed method.

Results and Discussion. The quantitative results are represented in Tab. 3 and Tab. 4. We observe that our contrastive diffusion achieves state-of-the-art performance for both general synthesis fidelity and input-output correspondence, and the *Sample-Inter* contrastive setting is more beneficial compared to *Step-Intra* for the image synthesis. This empirical finding again validates our assumption regarding the contrastive settings in Sec. 3.3, where the *Sample-Inter* setting helps more with the instance-level synthesis quality. Notably, as shown in Fig. 4 (right), our contrastive diffusion method shows model convergence at about 60 diffusion steps, while the vanilla version converges at approximately 100 steps on CUB200 Wah et al. (2011), which greatly increases the inference speed by 40%.

5 CONCLUSION

While DPMs have demonstrated remarkable potential, improving their training and inference efficiency while maintaining flexible and accurate results for conditional generation is an ongoing challenge, particularly for cross-modal tasks. Our Conditional Discrete Contrastive Diffusion (*CDCD*) loss addresses this by maximizing the mutual information between the conditioning input and the

generated output. Our contrastive diffusion mechanisms and negative sampling methods effectively incorporate this loss into DPM training. Extensive experiments on various cross-modal conditional generation tasks demonstrate the efficacy of our approach in bridging drastically differing domains.

ACKNOWLEDGMENTS

This research is partially supported by NSF SCH-2123521 and Snap unrestricted gift funding. This article solely reflects the opinions and conclusions of its authors and not the funding agents.

ETHICS STATEMENT.

As in other media generation works, there are possible malicious uses of such media to be addressed by oversight organizations and regulatory agencies. Our primary objective as researchers is always creating more reliable and secure AI and machine learning systems that maximally benefit our society.

REFERENCES

- Gunjan Aggarwal and Devi Parikh. Dance2music: Automatic dance-driven music generation. *arXiv preprint arXiv:2107.06252*, 2021.
- Peter Anderson, Xiaodong He, Chris Buehler, Damien Teney, Mark Johnson, Stephen Gould, and Lei Zhang. Bottom-up and top-down attention for image captioning and visual question answering. In *CVPR*, 2018.
- Relja Arandjelovic and Andrew Zisserman. Look, listen and learn. In *ICCV*, 2017.
- Jacob Austin, Daniel Johnson, Jonathan Ho, Daniel Tarlow, and Rianne van den Berg. Structured denoising diffusion models in discrete state-spaces. In *NeurIPS*, 2021.
- Yusuf Aytar, Carl Vondrick, and Antonio Torralba. Soundnet: Learning sound representations from unlabeled video. *NeurIPS*, 2016.
- Philip Bachman, R Devon Hjelm, and William Buchwalter. Learning representations by maximizing mutual information across views. In *NeurIPS*, 2019.
- Tadas Baltrušaitis, Chaitanya Ahuja, and Louis-Philippe Morency. Multimodal machine learning: A survey and taxonomy. *IEEE transactions on pattern analysis and machine intelligence*, 2018.
- Mohamed Ishmael Belghazi, Aristide Baratin, Sai Rajeshwar, Sherjil Ozair, Yoshua Bengio, Aaron Courville, and Devon Hjelm. Mutual information neural estimation. In *ICML*. PMLR, 2018.
- Jean-Pierre Briot, Gaëtan Hadjeres, and François-David Pachet. *Deep learning techniques for music generation*, volume 1. Springer, 2020.
- Z. Cao, G. Hidalgo Martinez, T. Simon, S. Wei, and Y. A. Sheikh. Openpose: Realtime multi-person 2d pose estimation using part affinity fields. *IEEE TPAMI*, 2019.
- Zhe Cao, Tomas Simon, Shih-En Wei, and Yaser Sheikh. Realtime multi-person 2d pose estimation using part affinity fields. In *CVPR*, 2017.
- Joao Carreira and Andrew Zisserman. Quo vadis, action recognition? a new model and the kinetics dataset. In *CVPR*, 2017.
- Ting Chen, Simon Kornblith, Mohammad Norouzi, and Geoffrey Hinton. A simple framework for contrastive learning of visual representations. In *ICLR*, 2020.
- Yu-Jie Chen, Shin-I Cheng, Wei-Chen Chiu, Hung-Yu Tseng, and Hsin-Ying Lee. Vector quantized image-to-image translation. In *ECCV*, 2022.
- Aiyu Cui, Daniel McKee, and Svetlana Lazebnik. Dressing in order: Recurrent person image generation for pose transfer, virtual try-on and outfit editing. In *CVPR*, 2021.

- Jia Deng, Wei Dong, Richard Socher, Li-Jia Li, Kai Li, and Li Fei-Fei. Imagenet: A large-scale hierarchical image database. In *CVPR*, 2009.
- Jacob Devlin, Ming-Wei Chang, Kenton Lee, and Kristina Toutanova. Bert: Pre-training of deep bidirectional transformers for language understanding. *arXiv preprint arXiv:1810.04805*, 2018.
- Prafulla Dhariwal and Alexander Nichol. Diffusion models beat gans on image synthesis. In *NeurIPS*, 2021.
- Prafulla Dhariwal, Heewoo Jun, Christine Payne, Jong Wook Kim, Alec Radford, and Ilya Sutskever. Jukebox: A generative model for music. *arXiv preprint arXiv:2005.00341*, 2020.
- Shangzhe Di, Zeren Jiang, Si Liu, Zhaokai Wang, Leyan Zhu, Zexin He, Hongming Liu, and Shuicheng Yan. Video background music generation with controllable music transformer. In *ACMMM*, 2021.
- Hao-Wen Dong, Wen-Yi Hsiao, Li-Chia Yang, and Yi-Hsuan Yang. Musegan: Multi-track sequential generative adversarial networks for symbolic music generation and accompaniment. In *AAAI*, 2018.
- Conor Durkan, Iain Murray, and George Papamakarios. On contrastive learning for likelihood-free inference. In *ICML*. PMLR, 2020.
- Daniel PW Ellis. Beat tracking by dynamic programming. *Journal of New Music Research*, 2007.
- Patrick Esser, Robin Rombach, Andreas Blattmann, and Bjorn Ommer. Imagebart: Bidirectional context with multinomial diffusion for autoregressive image synthesis. *NeurIPS*, 2021a.
- Patrick Esser, Robin Rombach, and Bjorn Ommer. Taming transformers for high-resolution image synthesis. In *CVPR*, 2021b.
- Chuang Gan, Deng Huang, Peihao Chen, Joshua B Tenenbaum, and Antonio Torralba. Foley music: Learning to generate music from videos. In *ECCV*, 2020a.
- Chuang Gan, Deng Huang, Hang Zhao, Joshua B Tenenbaum, and Antonio Torralba. Music gesture for visual sound separation. In *CVPR*, 2020b.
- Ruohan Gao, Tae-Hyun Oh, Kristen Grauman, and Lorenzo Torresani. Listen to look: Action recognition by previewing audio. In *CVPR*, 2020.
- Shuyang Gu, Dong Chen, Jianmin Bao, Fang Wen, Bo Zhang, Dongdong Chen, Lu Yuan, and Baining Guo. Vector quantized diffusion model for text-to-image synthesis. In *CVPR*, 2022.
- Kaiming He, Xiangyu Zhang, Shaoqing Ren, and Jian Sun. Deep residual learning for image recognition. In *CVPR*, 2016.
- Kaiming He, Haoqi Fan, Yuxin Wu, Saining Xie, and Ross Girshick. Momentum contrast for unsupervised visual representation learning. In *CVPR*, 2020.
- Jack Hessel, Ari Holtzman, Maxwell Forbes, Ronan Le Bras, and Yejin Choi. CLIPScore: a reference-free evaluation metric for image captioning. In *EMNLP*, 2021.
- Martin Heusel, Hubert Ramsauer, Thomas Unterthiner, Bernhard Nessler, and Sepp Hochreiter. Gans trained by a two time-scale update rule converge to a local nash equilibrium. *NeurIPS*, 2017.
- Jonathan Ho and Tim Salimans. Classifier-free diffusion guidance. *arXiv preprint arXiv:2207.12598*, 2022.
- Jonathan Ho, Ajay Jain, and Pieter Abbeel. Denoising diffusion probabilistic models. In *NeurIPS*, 2020.
- Jonathan Ho, Chitwan Saharia, William Chan, David J Fleet, Mohammad Norouzi, and Tim Salimans. Cascaded diffusion models for high fidelity image generation. *Journal of Machine Learning Research*, 2022.

- Emiel Hoogeboom, Didrik Nielsen, Priyank Jaini, Patrick Forré, and Max Welling. Argmax flows and multinomial diffusion: Towards non-autoregressive language models. *arXiv e-prints*, pp. arXiv-2102, 2021.
- Minghui Hu, Yujie Wang, Tat-Jen Cham, Jianfei Yang, and PN Suganthan. Global context with discrete diffusion in vector quantised modelling for image generation. *arXiv preprint arXiv:2112.01799*, 2021.
- Cheng-Zhi Anna Huang, Ashish Vaswani, Jakob Uszkoreit, Noam Shazeer, Ian Simon, Curtis Hawthorne, Andrew M Dai, Matthew D Hoffman, Monica Dinculescu, and Douglas Eck. Music transformer: Generating music with long-term structure. In *ICLR*, 2019.
- Chin-Wei Huang, Jae Hyun Lim, and Aaron C Courville. A variational perspective on diffusion-based generative models and score matching. In *NeurIPS*, 2021.
- Shulei Ji, Jing Luo, and Xinyu Yang. A comprehensive survey on deep music generation: Multi-level representations, algorithms, evaluations, and future directions. *arXiv preprint arXiv:2011.06801*, 2020.
- Will Kay, Joao Carreira, Karen Simonyan, Brian Zhang, Chloe Hillier, Sudheendra Vijayanarasimhan, Fabio Viola, Tim Green, Trevor Back, Paul Natsev, et al. The kinetics human action video dataset. *arXiv preprint arXiv:1705.06950*, 2017.
- Evangelos Kazakos, Arsha Nagrani, Andrew Zisserman, and Dima Damen. Epic-fusion: Audio-visual temporal binding for egocentric action recognition. In *ICCV*, 2019.
- Diederik P Kingma, Tim Salimans, Ben Poole, and Jonathan Ho. Variational diffusion models. In *NeurIPS*, 2021.
- Zhifeng Kong, Wei Ping, Jiaji Huang, Kexin Zhao, and Bryan Catanzaro. Diffwave: A versatile diffusion model for audio synthesis. In *ICLR*, 2020.
- Bruno Korbar, Du Tran, and Lorenzo Torresani. Cooperative learning of audio and video models from self-supervised synchronization. In *NeurIPS*, 2018.
- Kundan Kumar, Rithesh Kumar, Thibault de Boissiere, Lucas Gestin, Wei Zhen Teoh, Jose Sotelo, Alexandre de Brébisson, Yoshua Bengio, and Aaron C Courville. Melgan: Generative adversarial networks for conditional waveform synthesis. In *NeurIPS*, 2019.
- Junhyeok Lee and Seungu Han. Nu-wave: A diffusion probabilistic model for neural audio upsampling. *Proc. Interspeech 2021*, 2021.
- Bowen Li, Xiaojuan Qi, Thomas Lukasiewicz, and Philip Torr. Controllable text-to-image generation. In *NeurIPS*, 2019.
- Ruilong Li, Shan Yang, David A. Ross, and Angjoo Kanazawa. Ai choreographer: Music conditioned 3d dance generation with aist++. In *ICCV*, 2021.
- Tsung-Yi Lin, Michael Maire, Serge Belongie, James Hays, Pietro Perona, Deva Ramanan, Piotr Dollár, and C Lawrence Zitnick. Microsoft coco: Common objects in context. In *ECCV*. Springer, 2014.
- Yan-Bo Lin, Hung-Yu Tseng, Hsin-Ying Lee, Yen-Yu Lin, and Ming-Hsuan Yang. Exploring cross-video and cross-modality signals for weakly-supervised audio-visual video parsing. In *NeurIPS*, 2021.
- Matthew Loper, Naureen Mahmood, Javier Romero, Gerard Pons-Moll, and Michael J. Black. SMPL: A skinned multi-person linear model. *ACM Trans. Graphics (Proc. SIGGRAPH Asia)*, 34, 2015.
- Ilya Loshchilov and Frank Hutter. Decoupled weight decay regularization. *arXiv preprint arXiv:1711.05101*, 2017.
- Gautam Mittal, Jesse Engel, Curtis Hawthorne, and Ian Simon. Symbolic music generation with diffusion models. *arXiv preprint arXiv:2103.16091*, 2021.

- Alexander Quinn Nichol and Prafulla Dhariwal. Improved denoising diffusion probabilistic models. In *International Conference on Machine Learning*. PMLR, 2021.
- Aaron van den Oord, Oriol Vinyals, and Koray Kavukcuoglu. Neural discrete representation learning. In *NeurIPS*, 2017.
- Aaron van den Oord, Yazhe Li, and Oriol Vinyals. Representation learning with contrastive predictive coding. *arXiv preprint arXiv:1807.03748*, 2018.
- Andrew Owens and Alexei A Efros. Audio-visual scene analysis with self-supervised multisensory features. In *ECCV*, 2018.
- Andrew Owens, Jiajun Wu, Josh H McDermott, William T Freeman, and Antonio Torralba. Ambient sound provides supervision for visual learning. In *ECCV*, 2016.
- Alec Radford, Jong Wook Kim, Chris Hallacy, Aditya Ramesh, Gabriel Goh, Sandhini Agarwal, Girish Sastry, Amanda Askell, Pamela Mishkin, Jack Clark, et al. Learning transferable visual models from natural language supervision. In *ICML*. PMLR, 2021.
- Tanzila Rahman, Bicheng Xu, and Leonid Sigal. Watch, listen and tell: Multi-modal weakly supervised dense event captioning. In *ICCV*, 2019.
- Aditya Ramesh, Mikhail Pavlov, Gabriel Goh, Scott Gray, Chelsea Voss, Alec Radford, Mark Chen, and Ilya Sutskever. Zero-shot text-to-image generation. In *ICML*. PMLR, 2021.
- Ali Razavi, Aaron van den Oord, and Oriol Vinyals. Generating diverse high-fidelity images with vq-vae-2. In *NeurIPS*, 2019.
- Robin Rombach, Andreas Blattmann, Dominik Lorenz, Patrick Esser, and Björn Ommer. High-resolution image synthesis with latent diffusion models. In *CVPR*, 2022.
- Shulan Ruan, Yong Zhang, Kun Zhang, Yanbo Fan, Fan Tang, Qi Liu, and Enhong Chen. Dae-gan: Dynamic aspect-aware gan for text-to-image synthesis. In *ICCV*, 2021.
- Olga Russakovsky, Jia Deng, Hao Su, Jonathan Krause, Sanjeev Satheesh, Sean Ma, Zhiheng Huang, Andrej Karpathy, Aditya Khosla, Michael Bernstein, et al. Imagenet large scale visual recognition challenge. *IJCV*, 2015.
- Tim Sainburg, Marvin Thielk, and Timothy Q Gentner. Finding, visualizing, and quantifying latent structure across diverse animal vocal repertoires. *PLoS computational biology*, 16(10):e1008228, 2020.
- Jascha Sohl-Dickstein, Eric Weiss, Niru Maheswaranathan, and Surya Ganguli. Deep unsupervised learning using nonequilibrium thermodynamics. In *ICML*, 2015a.
- Jascha Sohl-Dickstein, Eric Weiss, Niru Maheswaranathan, and Surya Ganguli. Deep unsupervised learning using nonequilibrium thermodynamics. In *ICML*. PMLR, 2015b.
- Jiaming Song and Stefano Ermon. Multi-label contrastive predictive coding. In *NeurIPS*, 2020a.
- Jiaming Song and Stefano Ermon. Understanding the limitations of variational mutual information estimators. In *ICLR*, 2020b.
- Jiaming Song, Chenlin Meng, and Stefano Ermon. Denoising diffusion implicit models. In *ICLR*, 2020a.
- Yang Song and Stefano Ermon. Improved techniques for training score-based generative models. In *NeurIPS*, 2020c.
- Yang Song, Jascha Sohl-Dickstein, Diederik P Kingma, Abhishek Kumar, Stefano Ermon, and Ben Poole. Score-based generative modeling through stochastic differential equations. In *ICLR*, 2020b.
- Yang Song, Conor Durkan, Iain Murray, and Stefano Ermon. Maximum likelihood training of score-based diffusion models. In *NeurIPS*, 2021.

- Hongchen Tan, Xiuping Liu, Xin Li, Yi Zhang, and Baocai Yin. Semantics-enhanced adversarial nets for text-to-image synthesis. In *ICCV*, 2019.
- Ming Tao, Hao Tang, Songsong Wu, Nicu Sebe, Xiao-Yuan Jing, Fei Wu, and Bingkun Bao. Df-gan: Deep fusion generative adversarial networks for text-to-image synthesis. *arXiv preprint arXiv:2008.05865*, 2020.
- Yapeng Tian, Jing Shi, Bochen Li, Zhiyao Duan, and Chenliang Xu. Audio-visual event localization in unconstrained videos. In *ECCV*, 2018.
- Hung-Yu Tseng, Matthew Fisher, Jingwan Lu, Yijun Li, Vladimir Kim, and Ming-Hsuan Yang. Modeling artistic workflows for image generation and editing. In *ECCV*. Springer, 2020.
- Shuhe Tsuchida, Satoru Fukayama, Masahiro Hamasaki, and Masataka Goto. Aist dance video database: Multi-genre, multi-dancer, and multi-camera database for dance information processing. In *Proceedings of the 20th International Society for Music Information Retrieval Conference, (ISMIR)*, 2019.
- Arash Vahdat, Karsten Kreis, and Jan Kautz. Score-based generative modeling in latent space. In *Advances in Neural Information Processing Systems*, 2021.
- C. Wah, S. Branson, P. Welinder, P. Perona, and S. Belongie. The Caltech-UCSD Birds-200-2011 Dataset. Technical Report CNS-TR-2011-001, California Institute of Technology, 2011.
- Liwei Wang, Alexander Schwing, and Svetlana Lazebnik. Diverse and accurate image description using a variational auto-encoder with an additive gaussian encoding space. In *NeurIPS*, 2017.
- Xin Wang, Yuan-Fang Wang, and William Yang Wang. Watch, listen, and describe: Globally and locally aligned cross-modal attentions for video captioning. In *NAACL*, 2018.
- Yu Wu and Yi Yang. Exploring heterogeneous clues for weakly-supervised audio-visual video parsing. In *CVPR*, 2021.
- Yu Wu, Linchao Zhu, Yan Yan, and Yi Yang. Dual attention matching for audio-visual event localization. In *ICCV*, 2019.
- Yu Wu, Linchao Zhu, Xiaohan Wang, Yi Yang, and Fei Wu. Learning to anticipate egocentric actions by imagination. *IEEE TIP*, 30:1143–1152, 2021.
- Yu Wu, Lu Jiang, and Yi Yang. Switchable novel object captioner. *IEEE TPAMI*, 45(1):1162–1173, 2023. doi: 10.1109/TPAMI.2022.3144984.
- Tao Xu, Pengchuan Zhang, Qiuyuan Huang, Han Zhang, Zhe Gan, Xiaolei Huang, and Xiaodong He. Attngan: Fine-grained text to image generation with attentional generative adversarial networks. In *CVPR*, 2018.
- Zipeng Xu, Tianwei Lin, Hao Tang, Fu Li, Dongliang He, Nicu Sebe, Radu Timofte, Luc Van Gool, and Errui Ding. Predict, prevent, and evaluate: Disentangled text-driven image manipulation empowered by pre-trained vision-language model. *arXiv preprint arXiv:2111.13333*, 2021.
- Quanzeng You, Hailin Jin, Zhaowen Wang, Chen Fang, and Jiebo Luo. Image captioning with semantic attention. In *CVPR*, 2016.
- Han Zhang, Tao Xu, Hongsheng Li, Shaoting Zhang, Xiaogang Wang, Xiaolei Huang, and Dimitris N Metaxas. Stackgan: Text to photo-realistic image synthesis with stacked generative adversarial networks. In *CVPR*, 2017.
- Han Zhang, Tao Xu, Hongsheng Li, Shaoting Zhang, Xiaogang Wang, Xiaolei Huang, and Dimitris N Metaxas. Stackgan++: Realistic image synthesis with stacked generative adversarial networks. *IEEE TPAMI*, 2018.
- Han Zhang, Jing Yu Koh, Jason Baldridge, Honglak Lee, and Yinfei Yang. Cross-modal contrastive learning for text-to-image generation. In *CVPR*, 2021.

Minfeng Zhu, Pingbo Pan, Wei Chen, and Yi Yang. Dm-gan: Dynamic memory generative adversarial networks for text-to-image synthesis. In *CVPR*, 2019.

Ye Zhu, Yu Wu, Yi Yang, and Yan Yan. Describing unseen videos via multi-modal cooperative dialog agents. In *ECCV*, 2020.

Ye Zhu, Yu Wu, Hugo Latapie, Yi Yang, and Yan Yan. Learning audio-visual correlations from variational cross-modal generation. In *ICCAPS*, 2021a.

Ye Zhu, Yu Wu, Yi Yang, and Yan Yan. Saying the unseen: Video descriptions via dialog agents. In *TPAMI*, 2021b.

Ye Zhu, Kyle Olszewski, Yu Wu, Panos Achlioptas, Menglei Chai, Yan Yan, and Sergey Tulyakov. Quantized gan for complex music generation from dance videos. In *ECCV*, 2022a.

Ye Zhu, Yu Wu, Nicu Sebe, and Yan Yan. Vision+ x: A survey on multimodal learning in the light of data. *arXiv preprint arXiv:2210.02884*, 2022b.

We present more related work in Appendix A. Details about the theoretical deviation and training algorithms are included in Appendix B. In Appendix C, we describe additional experimental details and ablation analysis, including the resources required for training and inference. More qualitative examples are provided in Appendix D. Further discussions including the broader impact are included in Appendix E.

A MORE RELATED WORKS

In addition to the fields of *Diffusion Probabilistic Models*, *Contrastive Representation Learning*, and *VQ Representations for Conditional Generation* discussed in the main paper, our work is also closely related to the multi-modal learning and generation fields.

The research topic of multimodal learning, which incorporates data from various modalities such as audio, vision, and language has attracted much attention in recent years Baltrušaitis et al. (2018); Zhu et al. (2022b); Wu et al. (2023). General audio and visual learning works typically seek to investigate their correlations from the intrinsic synchronization nature Aytar et al. (2016); Korbar et al. (2018); Owens & Efros (2018); Owens et al. (2016); Arandjelovic & Zisserman (2017), and then utilize them in various downstream audio-visual tasks such as audio-visual action recognition Kazakos et al. (2019); Gao et al. (2020), audio-visual event localization and parsing Tian et al. (2018); Zhu et al. (2021a); Wu et al. (2019); Wu & Yang (2021), and audio-visual captioning Rahman et al. (2019); Wang et al. (2018). Works to generate music from visual or/and motion data have also been widely explored in recent years Gan et al. (2020a); Di et al. (2021); Aggarwal & Parikh (2021); Zhu et al. (2022a). For vision and language area, the text generation from visions are extensively explored in the image and video captioning task Zhu et al. (2020; 2021b); Anderson et al. (2018); You et al. (2016); Wang et al. (2017). At the same time, works on image/video generation from text have also attracted much attention with recently released largescale models Radford et al. (2021); Li et al. (2019); Ruan et al. (2021); Ramesh et al. (2021).

B DETAILED PROOF AND TRAINING

B.1 LOWER BOUND OF CDCD LOSS

We show that the proposed *CDCD* loss has a lower bound related to the mutual information and the number of negative samples N . The derivations below are similar to those from Oord et al. (2018):

$$\mathcal{L}_{\text{CDCD}} := \mathbb{E}_Z \left[-\log \frac{\frac{p_\theta(z_0|c)}{p_\theta(z_0)}}{\frac{p_\theta(z_0|c)}{p_\theta(z_0)} + \sum_{z^j \in Z'} \frac{p_\theta(z_0^j|c)}{p_\theta(z_0^j)}} \right] \quad (6a)$$

$$= \mathbb{E}_Z \log \left[1 + \frac{p_\theta(z_0)}{p_\theta(z_0|c)} \sum_{z^j \in Z'} \frac{p_\theta(z_0^j|c)}{p_\theta(z_0^j)} \right] \quad (6b)$$

$$\approx \mathbb{E}_Z \log \left[1 + N \frac{p_\theta(z_0)}{p_\theta(z_0|c)} \mathbb{E}_{Z'} \left[\frac{p_\theta(z_0^j|c)}{p_\theta(z_0^j)} \right] \right] \quad (6c)$$

$$= \mathbb{E}_Z \log \left[1 + N \frac{p_\theta(z_0)}{p_\theta(z_0|c)} \right] \quad (6d)$$

$$\geq \mathbb{E}_Z \log \left[N \frac{p_\theta(z_0)}{p_\theta(z_0|c)} \right] \quad (6e)$$

$$= \log(N) - I(z_0, c). \quad (6f)$$

B.2 CONVENTIONAL VARIATIONAL LOSS

The conventional variational loss \mathcal{L}_{vb} is derived as follows Sohl-Dickstein et al. (2015b):

$$\begin{aligned}
\mathcal{L}_{\text{vb}}(x) &:= \mathbb{E}_q[-\log \frac{p_\theta(x_{0:T})}{q(x_{1:T}|x_0)}] \\
&= \mathbb{E}_q[-\log p(x_T) - \sum_{t>1} \log \frac{p_\theta(x_{t-1}|x_t)}{q(x_t|x_{t-1})} - \log \frac{p_\theta(x_0|x_1)}{q(x_1|x_0)}] \\
&= \mathbb{E}_q[-\log p(x_T) - \sum_{t>1} \log \frac{p_\theta(x_{t-1}|x_t)}{q(x_{t-1}|x_t, x_0)} \cdot \frac{q(x_{t-1}|x_0)}{q(x_t|x_0)} - \log \frac{p_\theta(x_0|x_1)}{q(x_1|x_0)}] \\
&= \mathbb{E}_q[-\log \frac{p(x_T)}{q(x_T|x_0)} - \sum_{t>1} \log \frac{p_\theta(x_{t-1}|x_t)}{q(x_{t-1}|x_t, x_0)} - \log p_\theta(x_0|x_1)] \\
&= \mathbb{E}_q[D_{\text{KL}}(q(x_T|x_0)||p(x_T)) + \sum_{t>1} D_{\text{KL}}(q(x_{t-1}|x_t, x_0)||p_\theta(x_{t-1}|x_t)) - \log p_\theta(x_0|x_1)].
\end{aligned} \tag{7}$$

B.3 \mathcal{L}_{vb} WITH CONDITIONING PRIOR

Following the unconditional conventional variational loss, we then show its conditional variant with the conditioning c as prior, which has also been adopted in Gu et al. (2022).

$$\begin{aligned}
\mathcal{L}_{\text{vb}}(x, c) &= \mathcal{L}_0 + \mathcal{L}_1 + \dots + \mathcal{L}_{T-1} + \mathcal{L}_T \\
\mathcal{L}_0 &= -\log p_\theta(x_0|x_1, c) \\
\mathcal{L}_{t-1} &= D_{\text{KL}}(q(x_{t-1}|x_t, x_0)||p_\theta(x_{t-1}|x_t, c)) \\
\mathcal{L}_T &= D_{\text{KL}}(q(x_T|x_0)||p(x_T))
\end{aligned} \tag{8}$$

B.4 STEP-WISE AND SAMPLE-WISE CONTRASTIVE DIFFUSION

Below, we show the full derivation for the step-wise parallel contrastive diffusion loss. Given that the intermediate variables from $z_{1:T}$ are also taken into account in this step-wise contrastive diffusion, we slightly modify the initial notation $f(z_0, c) = \frac{p_\theta(z_0|c)}{p_\theta(z_0)}$ from Eq.(2) in the main paper to $f(z, c) = \frac{p_\theta(z_{0:T}|c)}{p_\theta(z_{0:T})}$.

$$\mathcal{L}_{\text{CDCD-Step}} := -\mathbb{E}_Z \left[\log \frac{f(z, c)}{f(z, c) + \sum_{z^j \in Z'} f(z^j, c)} \right] \tag{9a}$$

$$= \mathbb{E}_Z \log \left[1 + \frac{\sum_{z^j \in Z'} f(z^j, c)}{f(z, c)} \right] \tag{9b}$$

$$= \mathbb{E}_Z \log \left[1 + \frac{p_\theta(z_{0:T})}{p_\theta(z_{0:T}|c)} \sum_{z^j \in Z'} \frac{p_\theta(z_{0:T}^j|c)}{p_\theta(z_{0:T}^j)} \right] \tag{9c}$$

$$\approx \mathbb{E}_Z \log \left[1 + \frac{p_\theta(z_{0:T})}{p_\theta(z_{0:T}|c)} N \mathbb{E}_{Z'} \frac{p_\theta(z_{0:T}^j|c)}{p_\theta(z_{0:T}^j)} \right] \text{ (same as Eq.(6c))} \tag{9d}$$

$$\approx \mathbb{E}_Z \mathbb{E}_q \log \left[\frac{q(z_{1:T}|z_0)}{p_\theta(z_{0:T}|c)} N \frac{p_\theta(z_{0:T}|c)}{q(z_{1:T}|z_0)} \right] \text{ (conditional } p_\theta) \tag{9e}$$

$$\approx \mathbb{E}_q \left[-\log \frac{p_\theta(z_{0:T}|c)}{q(z_{1:T}|z_0)} \right] - \log N \mathbb{E}_{Z'} \mathbb{E}_q \left[-\log \frac{p_\theta(z_{0:T}|c)}{q(z_{1:T}|z_0)} \right] \tag{9f}$$

$$= \mathcal{L}_{\text{vb}}(z, c) - C \sum_{z^j \in Z'} \mathcal{L}_{\text{vb}}(z^j, c). \tag{9g}$$

Algorithm 1 Conditional Discrete Contrastive Diffusion Training. The referenced equations can be found in the main paper.

Input: Initial network parameters θ , contrastive loss weight λ , learning rate η , number of negative samples N , total diffusion steps T , conditioning information c , contrastive mode $m \in \{Step, Sample\}$.

```

1: for each training iteration do
2:    $t \sim Uniform(\{1, 2, \dots, T\})$ 
3:    $z_t \leftarrow Sample\ from\ q(z_t|z_{t-1})$ 
4:    $\mathcal{L}_{vb} \leftarrow \sum_{i=1, \dots, t} \mathcal{L}_i \triangleright Eq. 1$ 
5:   if  $m == Step$  then
6:     for  $j = 1, \dots, N$  do
7:        $z_t^j \leftarrow Sample\ from\ q(z_t^j|z_{t-1}^j, c) \triangleright$  from negative variables in previous steps
8:     end for
9:      $\mathcal{L}_{CDCD} = -\frac{1}{N} \sum \mathcal{L}_{vb}^j \triangleright Eq. 3$ 
10:  else if  $m == Sample$  then
11:    for  $j = 1, \dots, N$  do
12:       $z_t \leftarrow Sample\ from\ q(z_t|z_0^j, c) \triangleright$  from negative variables in step 0
13:    end for
14:     $\mathcal{L}_{CDCD} = -\frac{1}{N} \sum \mathcal{L}_{z_0}^j \triangleright Eq. 4$ 
15:  end if
16:   $\mathcal{L} \leftarrow \mathcal{L}_{vb} + \lambda \mathcal{L}_{CDCD} \triangleright Eq. 5$ 
17:   $\theta \leftarrow \theta - \eta \nabla_{\theta} \mathcal{L}$ 
18: end for

```

In the above Eq.(9g), C stands for a constant that equals to $\log N$, which can be further adjusted by the weight we select for the $CDCD$ loss as in Eq. 5.

Similarly for the sample-wise auxiliary contrastive diffusion, the loss can be derived as follows:

$$\mathcal{L}_{CDCD-Sample} := -\mathbb{E}_Z \left[\log \frac{f(z_0, c)}{f(z_0, c) + \sum_{z^j \in Z'} f(z_0^j, c)} \right] \quad (10a)$$

$$= \mathbb{E}_Z \log \left[1 + \frac{p_{\theta}(z_0)}{p_{\theta}(z_0|c)} N \mathbb{E}_{Z'} \left[\frac{p_{\theta}(z_0^j|c)}{p_{\theta}(z_0^j)} \right] \right] \quad (10b)$$

$$\approx \mathbb{E}_Z \mathbb{E}_q \log \left[\frac{q(z_{1:T}|z_0)}{p_{\theta}(z_0|c)} N \frac{p_{\theta}(z_0|c)}{q(z_{1:T}|z_0)} \right] \quad (10c)$$

$$\approx \mathbb{E}_q \left[-\log \frac{p_{\theta}(z_0|c)}{q(z_{1:T}|z_0)} \right] - N \mathbb{E}_{Z'} \mathbb{E}_q \left[-\log \frac{p_{\theta}(z_0|c)}{q(z_{1:T}|z_0)} \right] \quad (10d)$$

$$= \mathbb{E}_q \left[-\log p_{\theta}(z_0|z_t, c) \right] - C \sum_{z^j \in Z'} \mathbb{E}_q \left[-\log p_{\theta}(z_0^j|z_t, c) \right]. \quad (10e)$$

Note that from a high-level perspective, our contrastive idea covers two different concepts, while conventional contrastive learning usually focuses only on the negative samples. In our case, due to the unique formulation of diffusion models that bring the diffusion steps into the methodology design, we consider the contrast within the context of “negative samples” and “negative steps” (also corresponds to the “negative intermediate steps”). In the deviation above, we use the symbols Z and q to distinguish between these two concepts.

B.5 CONDITIONAL DISCRETE CONTRASTIVE DIFFUSION TRAINING

The training process for the proposed contrastive diffusion is explained in Algo. 1.

C ADDITIONAL EXPERIMENTAL DETAILS AND ANALYSIS

C.1 DANCE-TO-MUSIC TASK

Implementation. The sampling rate for all audio signals is 22.5 kHz in our experiments. We use 2-second music samples as in Zhu et al. (2022a) for our main experiments, resulting in 44,100 audio

data points for each raw music sequence. For the Music VQ-VAE, we fine-tuned Jukebox Dhariwal et al. (2020) on our data to leverage its pre-learned codebook from a large-scale music dataset (approximately 1.2 million songs). The codebook size K is 2048, with a token dimension $d_z = 128$, and the hop-length L is 128 in our default experimental setting. For the motion module, we deploy a backbone stacked with convolutional layers and residual blocks. The dimension size of the embedding we use for music conditioning is 1024. For the visual module, we extract I3D features Carreira & Zisserman (2017) using a model pre-trained on Kinetics Kay et al. (2017) as the visual conditioning information, with a dimension size of 2048. In the implementation of our contrastive diffusion model, we adopt a transformer-based backbone to learn the denoising network p_θ . It includes 19 transformer blocks, in which each block consists of full-attention, cross-attention and a feed-forward network, and the channel size for each block is 1024. We set the initial weight for the contrastive loss as $\lambda = 5e - 5$. The numbers of intra- and inter-negative samples for each GT music sample are both 10. The AdamW Loshchilov & Hutter (2017) optimizer with $\beta_1 = 0.9$ and $\beta_2 = 0.96$ is deployed in our training, with a learning rate of $4.5e - 4$. We also employ an adaptive weight for the denoising loss weight by gradually decreasing the weight as the diffusion step increases and approaches the end of the chain. The visual module, motion module, and the contrastive diffusion model are jointly optimized. The architecture of adopted motion encoder is shown in Tab. 5, which is the same as in Zhu et al. (2022a).

Table 5: Architecture for the motion encoder.

6×1 , stride=1, Conv 256, LeakyReLU
Residual Stack 256
3×1 , stride=1, Conv 512, LeakyReLU
Residual Stack 512
3×1 , stride=1, Conv 1024, LeakyReLU
Residual Stack 1024
3×1 , stride=1, Conv 1024, LeakyReLU
4×1 , stride=1, Conv 1

Other than the aforementioned implementation details, we also include the mask token technique that bears resemblance to those used in language modelling Devlin et al. (2018) and text-to-image synthesis Gu et al. (2022) for our dance-to-music generation task. We adopt a truncation rate of 0.86 in our inference.

MOS Evaluation Test. We asked a total of 32 participants to participate in our subjective Mean Opinion Scores (MOS) music evaluations Zhu et al. (2022a); Kumar et al. (2019), among which 11 of them are female, while the rest are male. For the dance-music coherence test, we fuse the generated music samples with the GT videos as post-processing. We then asked each evaluator to rate 20 generated videos with a score of 1 (least coherent) to 5 (most coherent) after watching the processed video clip. Specifically, the participants are asked to pay more attention to the dance-music coherence in terms of the dance moves corresponding to the music genre and rhythm, rather than the overall music quality, with reference to the GT video clips with the original music. As for the overall quality evaluations, we only play the audio tracks without the video frames to each evaluator. As before, they are asked to rate the overall music quality with a score of 1 (worst audio quality) to 5 (best audio quality).

Training Cost. For the dance2music task experiments on the AIST++ dataset, we use 4 NVIDIA RTX A5000 GPUs, and train the model for approximately 2 days. For the same task on the TikTok dance-music dataset, the training takes approximately 1.5 days on the same hardware.

Complete Results for Contrastive Settings. As discussed in our main paper, there are four possible combinations for contrastive settings given different contrastive diffusion mechanisms and negative sampling methods. Here, we include complete quantitative scores for different contrastive settings in Tab. 6. We observe that all the four contrastive settings, including the *Step-Inter* and *Sample-Intra* settings that are not reported in our main paper, help to improve the performance. As we noted, amongst all the settings, *Step-Intra* and *Sample-Inter* are more reasonable and yield larger improvements for intra-sample data attributes (*i.e.*, beats scores) and instance-level features (*i.e.*, genre accuracy scores).

Table 6: Complete quantitative evaluation results for the dance-to-music generation task on the AIST++ dataset. We report the mean and standard deviations of our contrastive diffusion for three inference tests.

Musical features	Rhythms	Rhythms	Genre	Coherence	Quality
Metrics	Coverage \uparrow	Hit \uparrow	Accuracy \uparrow	MOS \uparrow	MOS \uparrow
GT Music	100	100	88.5	4.7	4.8
Foley Gan et al. (2020a)	74.1	69.4	8.1	2.9	-
Dance2Music Aggarwal & Parikh (2021)	83.5	82.4	7.0	3.0	-
CMT Di et al. (2021)	85.5	83.5	11.6	3.0	-
D2M-GAN Zhu et al. (2022a)	88.2	84.7	24.4	3.3	3.4
Ours Vanilla	89.0 \pm 1.1	83.8 \pm 1.5	25.3 \pm 0.8	3.3	3.6
Ours Step-Intra	93.9 \pm 1.2	90.7 \pm 1.5	25.8 \pm 0.6	3.6	3.5
Ours Step-Inter	92.4 \pm 1.0	88.9 \pm 1.7	24.3 \pm 0.7	3.4	3.5
Ours Sample-Intra	91.5 \pm 1.7	84.6 \pm 1.6	26.0 \pm 0.8	3.5	3.6
Ours Sample-Inter	91.8 \pm 1.6	86.9 \pm 1.4	27.2 \pm 0.5	3.6	3.6

Table 7: Ablation results for different music lengths on the AIST++ dataset.

Length	Methods	Beats Coverage \uparrow	Beats Hit \uparrow	Genre Acc. \uparrow
2s	D2M-GAN Zhu et al. (2022a)	88.2	84.7	24.4
	Ours Vanilla	89.0	83.8	25.3
	Ours Step-Intra	93.9	90.7	25.8
	Ours Sample-Inter	91.8	86.9	27.2
4s	D2M-GAN Zhu et al. (2022a)	87.1	83.0	23.3
	Ours Vanilla	86.2	81.8	24.6
	Ours Step-Intra	93.1	86.4	25.3
	Ours Sample-Inter	91.4	83.9	26.1
6s	D2M-GAN Zhu et al. (2022a)	-	-	-
	Ours Vanilla	84.8	81.1	22.7
	Ours Step-Intra	87.9	83.2	22.9
	Ours Sample-Inter	86.3	81.6	23.0

Ablation on Music Length. Although we use 2-second musical sequences in the main experiments to make for consistent and fair comparisons with Zhu et al. (2022a), our framework can also synthesize longer musical sequences. In the supplementary, we show our generated music sequences in 6-seconds. The quantitative evaluations in terms of different musical sequence lengths are presented Tab. 7, where we show better performance when synthesizing longer musical sequences.

C.2 TEXT-TO-IMAGE TASK

Implementation. For the text-to-image generation task, we adopt VQ-GAN Esser et al. (2021b) as the discrete encoder and decoder. The codebook size K is 2886, with a token dimension $d_z = 256$. VQ-GAN converts a 256×256 resolution image to 32×32 discrete tokens. For the textual conditioning, we employ the pre-trained CLIP Radford et al. (2021) model to encode the given textual descriptions. The denoising diffusion model p_θ has 18 transformer blocks and a channel size of 192, which is a similar model scale to the small version of VQ-Diffusion Gu et al. (2022). We use $\lambda = 5e - 5$ as the contrastive loss weight. Similar to the dance-to-music task, we also use the adaptive weight that changes within the diffusion stages. We keep the same truncation rate of 0.86 as in our dance-to-music experiment and in Gu et al. (2022). Unlike in the dance-to-music experiments, where we jointly learn the conditioning encoders, both the VQ-GAN and CLIP models are fixed during the contrastive diffusion training.

Training Cost. For the text2image task experiments on the CUB200 dataset, the training takes approximately 5 days using 4 NVIDIA RTX A5000 GPUs. For the same experiments on the MSCOCO dataset, we run the experiments on Amazon Web Services (AWS) using 8 NVIDIA Tesla V100 GPUs. This task required 10 days of training.

Table 8: Comparisons in terms of the task, datasets, model scale, and training time between our proposed CDCD and some other diffusion-based works.

Tasks	Dataset	Method	Param.	Training time
Dance-to-Music	AIST++ Li et al. (2021)	Ours CDCD	350M	8 V100 days
Dance-to-Music	TikTok Zhu et al. (2022a)	Ours CDCD	350M	6 V100 days
Text-to-Image	CUB200 Wah et al. (2011)	Ours CDCD	35M	20 V100 days
Text-to-Image	MSCOCO Lin et al. (2014)	Ours CDCD	35M	80 V100 days
Class-conditioned Image Synthesis	ImageNet	Ours CDCD	370 M	160 V100 days
Image Synthesis	ImageNet	ADMDhariwal & Nichol (2021)	-	150-1000 V100 days
Image Synthesis	ImageNet	LDM Rombach et al. (2022)	400M	270 V100 days

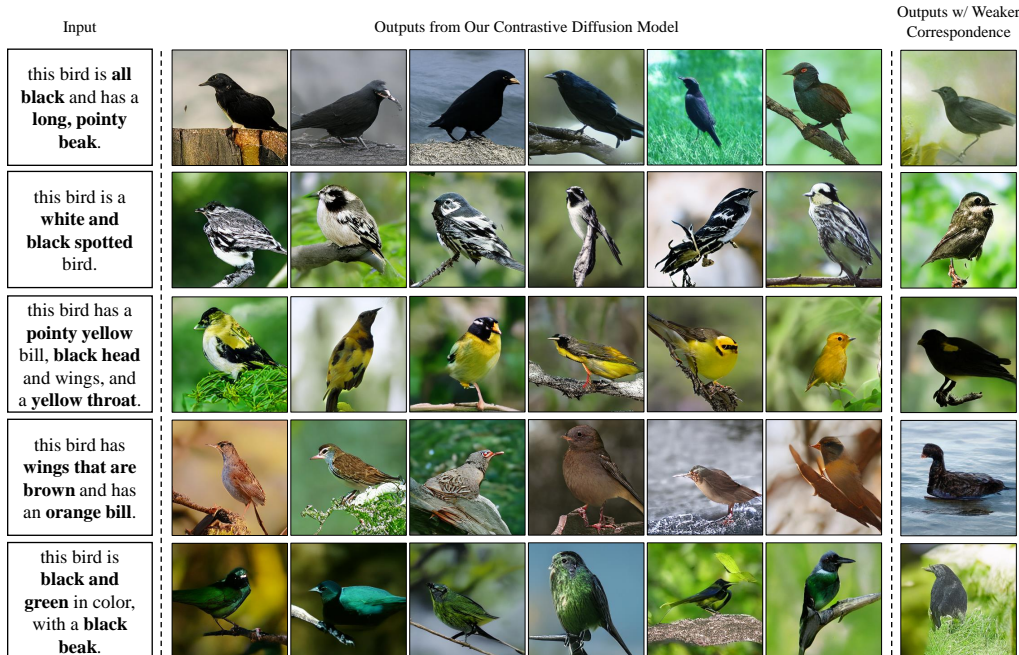


Figure 5: More qualitative results from our text-to-image experiments on CUB200 dataset. We show examples of the text input (left column), the synthesized images from our contrastive diffusion model with 80 diffusion steps and a FID score of 12.61 (middle column), and the output from existing method Gu et al. (2022) with 100 diffusion steps and a FID score 12.97.

C.3 CLASS-CONDITIONED IMAGE SYNTHESIS TASK

Implementation. For the class-conditioned image synthesis, we also adopt the pre-trained VQ-GAN Esser et al. (2021b) as the discrete encoder and decoder. We replace the conditioning encoder with class embedding optimized during the contrastive diffusion training. The size of the conditional embedding is 512. Other parameters and techniques remain the same, as in the text-to-image task.

Training Cost. For the class-conditioned experiments on the ImageNet, we use 8 NVIDIA Tesla V100 GPUs running on AWS. This task required 20 days of training.

D MORE QUALITATIVE RESULTS

D.1 GENERATED MUSIC SAMPLES

For qualitative samples of synthesized dance music sequences, please refer to our anonymous page in the supplement with music samples. In addition to the generated music samples on AIST++ Tsuchida et al. (2019); Li et al. (2021) and TikTok Dance-Music Dataset Zhu et al. (2022a), we also include some qualitative samples obtained with the music editing operations based on the dance-music genre



Figure 6: More qualitative results from our text-to-image experiments on COCO dataset. We show examples of the text input (left column), the synthesized images from our contrastive diffusion model with 80 diffusion steps and a FID score of 28.76 (middle column), and the output from existing method Gu et al. (2022) with 100 diffusion steps and a FID score 30.17.

annotations from AIST++. Specifically, we edit the original paired motion conditioning input with a different dance-music genre using a different dance choreographer.

Discussion on Musical Representations and Audio Quality. It is worth noting that we only compare the overall audio quality with that of D2M-GAN Zhu et al. (2022a). This is due to the nature of the different musical representations in the literature of deep-learning based music generation Gan et al. (2020a); Dong et al. (2018); Huang et al. (2019); Gan et al. (2020b); Aggarwal & Parikh (2021). There are mainly two categories for adopted musical representations in previous works: pre-defined symbolic and learning-based representations Ji et al. (2020); Briot et al. (2020). For the former symbolic music representation, typical options include 1D piano-roll and 2D MIDI-based representations. While these works benefit from the pre-defined music synthesizers and produce music that does not include raw audio noise, the main limitation is that such representations are usually limited to a

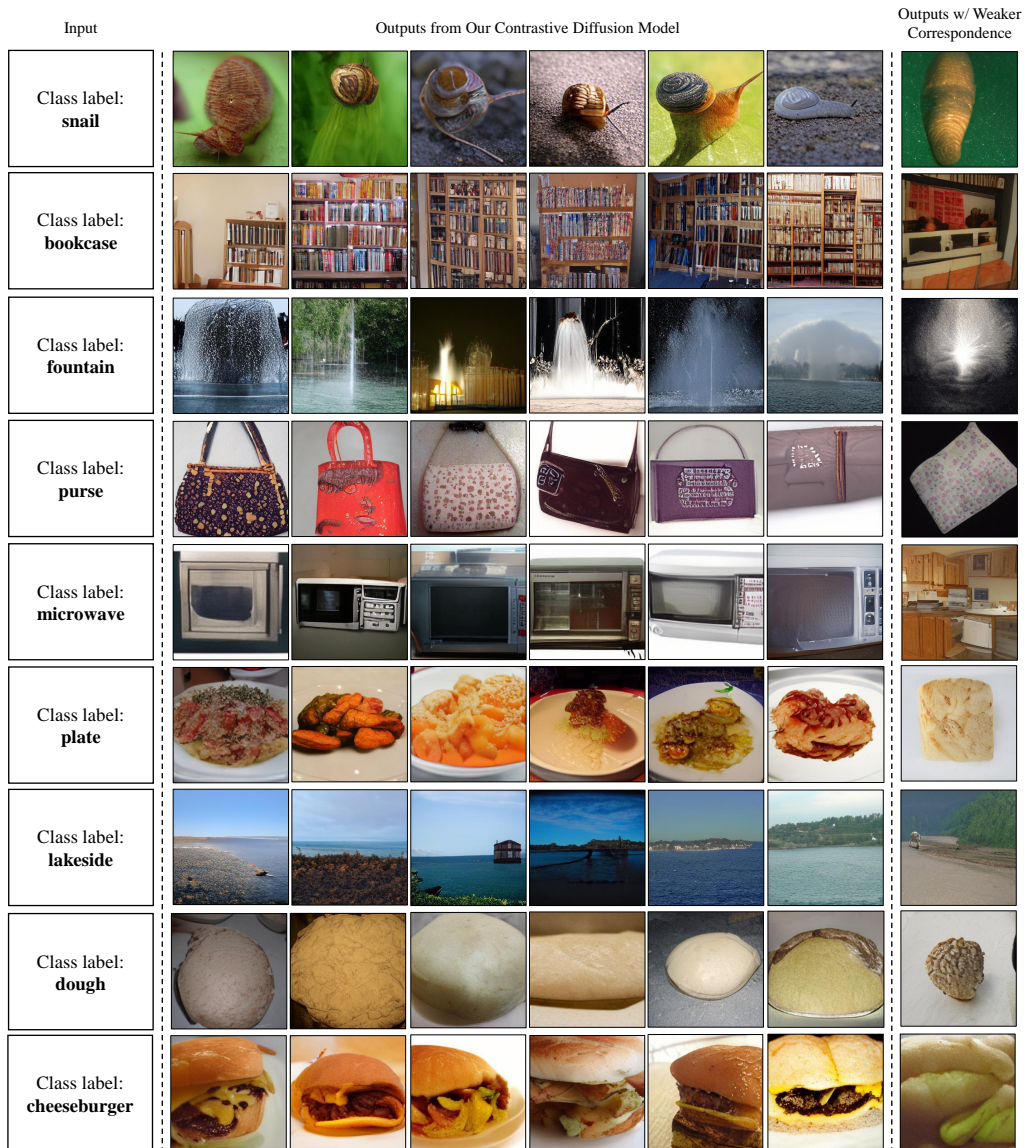


Figure 7: More qualitative results from our class-conditioned image synthesis experiments on ImageNet. We show examples of the text input (left column), the synthesized images from our contrastive diffusion model with 80 diffusion steps and a FID score of 11.74 (middle column), and the output from existing method Gu et al. (2022) with 100 diffusion steps and a FID score 11.89.

single specific instrument, which hinders their flexibility to be applied in wider and more complex scenarios such as dance videos. In contrast, the learning-based music representations (*i.e.*, musical VQ in our case) rely on well-trained music synthesizers as decoders, but can be used as a unified representation for various musical sounds, *e.g.*, instruments or voices. However, the training of such music encoders and decoders for high-quality audio signals itself remains a challenging problem. Specifically, high-quality audio is a form of high-dimensional data with an extremely large sampling rate, even compared to high-resolution images. For example, the sampling rate for CD-quality audio signals is 44.1 kHz, resulting in 2,646,000 data points for a one-minute musical piece. To this end, existing deep learning based works Dhariwal et al. (2020); Kumar et al. (2019) for music generation employ methods to reduce the number of dimensions, *e.g.*, by introducing hop lengths and a smaller

sampling rate. These operations help to make music learning and generation more computationally tractable, but also introduce additional noise in the synthesized audio signals.

In this work, we adopt the pre-trained JukeBox model Dhariwal et al. (2020) as our music encoder and decoder for the musical VQ representation. The adopted model has a hop length of 128, which corresponds to the top-level model from their original work Dhariwal et al. (2020). Jukebox employs 3 models: top-, middle-, and bottom-level, with both audio quality and required computation increasing from the first to the last model. As an example, in the supplemental HTML page, we provide music samples directly reconstructed from JukeBox using the top-level model we employ in our work, compared to the ground-truth audio. While they allow for high-quality audio reconstruction (from the bottom-level model, with a hop length of 8), it requires much more time and computation not only for training but also for the final inference, *e.g.*, 3 hours to generate a 20-second musical sequence. As the synthesized music from the top-level model includes some audible noise, we apply a noise reduction operation Sainburg et al. (2020). However, the overall audio quality is not a primary factor that we specifically address in this work on cross-modal conditioning and generation, as it largely depends on the specific music encoder and decoder that are employed. This explains why we report similar MOS scores in terms of the general audio quality.

D.2 SYNTHESIZED IMAGES

We present more qualitative examples for text-to-image synthesis and class-conditioned image synthesis in Fig. 5, Fig. 6, and Fig. 7.

E FURTHER DISCUSSION ON THE CDCD LOSS

In this section, we provide our further discussion on the proposed *CDCD* loss in terms of various aspects, including its relevance to the existing auxiliary losses, the impact of the *CDCD* strength, as well as additional experimental results.

E.1 CDCD AS AUXILIARY LOSS

While the diffusion models are typically trained and optimized with the conventional variational lower bound loss L_{vb} as we described in the main paper and Appendix B.2, there are several different types of auxiliary losses proposed to further regularize and improve the learning of diffusion models. Specifically, Dhariwal & Nichol (2021) introduces the idea of classifier based guidance for the diffusion denoising probabilistic models with continuous state space. Classifier-free guidance is proposed in Ho & Salimans (2022). In the area with discrete diffusion formulations Austin et al. (2021); Gu et al. (2022), an auxiliary loss that encourages the model to predict the noiseless token at the arbitrary step is adopted and proven to help with the synthesis quality.

Similar to the previous cases, we consider the proposed *CDCD* loss as a type of auxiliary losses, which seeks to provide additional guidance to better learn the conditional distribution $p(x|c)$. Specifically, the classifier-free guidance Ho & Salimans (2022) propose to randomly discard conditioning while learning a conditional diffusion generative model, which bears resemblance to our introduced downsampled contrastive steps in Appendix E.3.

E.2 IMPACT OF CDCD STRENGTH

We further show the ablation studies on the parameter λ , which is the weight of our proposed *CDCD* loss that characterize the strength of this contrastive regularizer.

We conduct the dance-to-music generation experiments with different values of λ , and show the results in Tab. 9. As we observe from the table that the performance in terms of the beat scores are relatively robust for different λ values ranging from $4e - 5$ to $5e - 5$. At the same time, we empirically observe that with a large value of λ , the model converges faster with less training epochs.

In case of the image synthesis task, we are rather cautious on the strength of the imposed contrastive regularizer. Intuitively, the proposed *CDCD* loss encourages the model to learn a slightly different distribution for negative samples, which could impose a trade-off between the one for the actual data given a specific conditioning. Therefore, while a larger value of λ helps with the learning speed, we

Table 9: Ablation results in terms of λ on the dance-to-music task.

Value	Beats Coverage	Beats Hit
$5e-4$	93.4	90.2
$1e-5$	93.3	91.0
$5e-5$	93.9	90.7

Table 10: Ablation results in terms of λ on the dance-to-music task.

Method	Beats Coverage	Beats Hit
Full ($T_c = 100$)	93.9	90.7
$T_c = 80$	93.4	90.5
$T_c = 60$	92.7	90.4

empirically set the λ to be $5e - 5$. Note that this value is adapted from the weight for other auxiliary losses in previous works Gu et al. (2022).

E.3 DOWNSAMPLED CONTRASTIVE STEPS

While we show the performance of complete *step-wise* contrastive diffusion in the main paper, we discuss here an alternative way to implement the proposed method with less computational cost, by downsampling the contrastive steps in the diffusion process. Specifically, we randomly downsampled the steps with the proposed *CDCD* loss, which shares the similar spirit as in the class-free guidance Ho & Salimans (2022) to randomly drop out the conditioning. The experimental results are listed in Tab. 10, where there is little performance drop with downsampled contrastive steps.